".

Estimation of Biogenic Volatile Organic Compounds (BVOCs) Emissions in Forest Ecosystems Using Drone-Based LiDAR, Photogrammetry, and Image Recognition Technologies

Xianzhong Duan[1,#], Ming Chang[1,#,*], Guotong Wu[1], Suping Situ[2], Shengjie Zhu[3], Qi Zhang[4], Yibo Huangfu[1], Weiwen Wang[1], Weihua Chen[1], Bin Yuan[1], and Xuemei Wang[1]

[1]College of Environment and Climate, Institute for Environmental and Climate Research, Guangdong-Hongkong-Macau Joint Laboratory of Collaborative Innovation for Environmental Quality, Jinan University, Guangzhou, China
[2]Foshan Ecological and Environmental Monitoring Station of Guangdong Province, Foshan, China
[3]Department of Environmental Science, Guangdong Polytechnic of Environmental Protection Engineering, Foshan, China
[4]Tianjin Academy of Eco-environmental Science, Tianjin, China
[#]These authors contributed equally to this work.

Correspondence: Ming Chang (changming@email.jnu.edu.cn)

Abstract.

Biogenic volatile organic compounds (BVOCs), as a crucial component that impacts atmospheric chemistry and ecological interactions with various organisms, play a significant role in the atmosphere-ecosystem relationship. However, traditional field observation methods are challenging to accurately estimate BVOCs emissions in forest ecosystems with high biodiversity, leading to significant uncertainty in quantifying these compounds. To address this issue, this research proposes a workflow utilizing drone-mounted LiDAR and photogrammetry technologies for identifying plant species to obtain accurate BVOCs emissions data. By applying this workflow to a typical subtropical forest plot, the following findings were made: The drone-mounted LiDAR and photogrammetry modules effectively segmented trees and acquired single wood structures and images of each tree. Image recognition technology enabled relatively accurate identification of tree species, with the highest frequency family being Euphorbiaceae. The largest cumulative isoprene emissions in the study plot were from the Myrtaceae family while monoterpenes were from the Rubiaceae family. To fully leverage the estimation results of BVOCs emissions directly from individual tree levels, it may be necessary for communities to establish more comprehensive tree species emission databases and models.

1 Introduction

Biogenic volatile organic compounds (BVOCs) is the medium of communication for plants to realize their wide ecological functions (Laothawornkitkul et al., 2009). BVOCs are involved in plant growth, reproduction and defense (Peñuelas and Staudt, 2010). Plants respond to the feeding of herbivores by emitting BVOCs to attract potential predators or as repellents (Kegge and Pierik, 2010). The communication process between plants is also based on BVOCs (Šimpraga et al., 2016). For example, gnawed plants will emit BVOCs to induce the production of defensive substances in non-attack objects (Dicke and Baldwin, 2010). In addition, BVOCs components are also used by plants to attract pollinators to bloom (Loreto et al., 2014). For the plants themselves, under heat waves or high ozone concentrations, BVOCs seem to reduce oxidative stress and other stresses caused by the complex non-biological urban environment (Ghirardo et al., 2016; Chen et al., 2018). At the same time, BVOCs are emitted into the atmosphere from vegetation and have significant impacts on other organisms and atmospheric chemistry and physics (Peñuelas and Staudt, 2010). BVOCs account for 90% of VOCs in atmospheric chemistry research which were considered as the fuel to drive atmospheric chemical processes and the key component of the atmosphere (Heald and Kroll, 2020). The atmospheric chemical activity of BVOCs species is very sprightly, and it's lifetime usually from only a few minutes to a few hours (Mellouki et al., 2015; Canaval et al., 2020). The contribution of BVOCs emission to global secondary organic aerosol (SOA) generation is about 90%, which is the main source of global atmospheric SOA (Henze et al., 2008). At the same time, BVOCs contributed about 10% $\sim$ 30% of the surface ozone in urban areas (Ran et al., 2011; Tsimpidi et al., 2012; Wu et al., 2020; Chen et al., 2022).

However, there is considerable uncertainty in the estimation of BVOCs (about 90% $\sim$ 120%) which constrains our understanding of the atmospheric environment and ecological effects of BVOCs (Situ et al., 2014; Wang et al., 2021). Especially for the forest ecosystem with the highest biodiversity, forest vegetation is considered to be the main contributer of BVOCs emissions, accounting for more than 70% of global BVOCs emissions, but the uncertainty of estimation of BVOCs emissions from forest vegetation is the most significant (Hartley et al., 2017). This uncertainty arises from two aspects: the lack of field observations and the simplification of numerical simulations. There are different methods for measuring BVOCs emissions on various scales. At the leaf and plant scale, scholars have used confined chamber and various improved confined chamber methods (for example, open-top chamber, free air concentration enrichment, etc) to conduct a large number of outstanding observational studies on the BVOCs emissions of leaves, branches and the whole tree and contribute different BVOCs database of single-tree BVOCs component emissions (Isidorov et al., 1990; Komenda and Koppmann, 2002; Baghi et al., 2012; Curtis et al., 2014). Existing potential BVOCs emission databases include seBVOCs(Steinbrecher et al., 2009), the tree BVOCs index(Simpson and McPherson, 2011), MEGAN(Guenther et al., 2012), and other general inventories (e.g. http://itreetools.org/; http://www.es.lancs.ac.uk/cnhgroup/download.html), etc. These studies mainly quantify the emission rate of BVOCs from specific tree species, which can help understand the processes and factors that affect the emission of BVOCs. At the forest landscape and canopy scale, flux towers are generally established at specific forest sites to observe the BVOCs emissions of the entire vegetation canopy (Sarkar et al., 2020). This method is relatively reliable and widely used, and can estimate the vegetation canopy emission flux within a range of several hundred meters from the flux tower. The closed chamber method and flux tower observation results can indirectly calculate the BVOC emission flux at ecological scales with low biodiversity, but for ecosystems with high biodiversity, such as tropical rainforest areas, this method is difficult to characterize the characteristics of all species.

In order to bypass the detailed investigation of ecosystem species, the academic community used aerial surveys and satellite remote sensing methods for indirect inversion of the emissions flux of BVOCs at the ecosystem and regional scales(Batista et al., 2019). However, its inversion accuracy is relatively low and there are still significant errors. Similarly, due to the chemical composition of BVOCs and the diversity of their emitting tree species, as well as the influence of many environmental factors on the emission process of BVOCs, accurately simulating BVOC emissions using numerical models faces significant challenges. Existing numerical models (for example, BEIS, g95, MEGAN, BEM, etc.) mainly use land use, leaf biomass, emission factors, and meteorological elements to estimate BVOCs emitted by vegetation (Wang et al., 2016; Chen et al., 2022). And the key source of uncertainty in its estimation comes from the inaccuracy of the numerical model on the parameterazation and characterization of land use types, forest tree species composition, and leaf biomass. Recent studies have found significant spatial heterogeneity of BVOCs at the sub forest scale (e.g. hundreds of meters on mountain slopes)(Li et al., 2021). Due to differences in the distribution of forest tree species, their BVOCs emissions are more complex than commonly assumed in biosphere emission models. Overall, for the calculation of BVOCs emissions, accurately characterizing the spatial distribution of emission factors is a scientific challenge that need be overcome to accurately quantify the spatial distribution of BVOCs emissions.

In recent years, consumer-grade UAV platforms, LiDAR measurement technology and computer image recognition technology have developed rapidly. UAVs equipped with measuring instruments for rapid sample observation technology gradually mature, and its positioning accuracy can reach the centimeter level. Even in areas such as forest protection areas, it is possible to set up routes to carry out surveys based on suitable forest gaps. UAVs equipped with sensors to measure atmospheric components have also begun to emerge (Villa et al., 2016). Many scholars install sensors in drone-based platforms for low-cost and flexible measurement of VOC, black carbon (BC), ozone, aerosol particles, etc (Brosy et al., 2017; Rüdiger et al., 2018; Shakhatreh et al., 2019; Li et al., 2021; Wu et al., 2021). And the camera carried by the drone can also obtain very high-resolution images, and even multi-spectral images (Nebiker et al., 2008; Villa et al., 2016; Dash et al., 2017). At the same time, the miniaturization of LiDAR measurement technology also makes it possible to be carried by UAVs (Zhao et al., 2016). As the most accurate surveying instrument to date, LiDAR can revolutionary characterize the canopy structure of each tree in the measurement range by obtaining point clouds compared to existing measurement methods. (Li et al., 2012; Jin et al., 2021). The characterization of forest community structure, morphological and physiological forest traits has been greatly enriched by the combined laser scanning and imaging spectroscopy (Schneider et al., 2017).

The recognition of plant species has undergone rapid development with computer image recognition technology. (Fassnacht et al., 2016; Cheng et al., 2023). Usually, machine learning and deep learning methods are used to call plant image libraries to train machine vision interpretation learning models, and then violently interpret high-resolution multi-spectral remote sensing images and laser point clouds to obtain accurate plant populations and species result (Sylvain et al., 2019). At present, there are several vegetation species classifiers have been applied: logistic regression, linear discriminat analysis, random forest, support vector machines, k-nearest neighbors (kNN), and 2d or 3d convolutional neural networks (CNNs) (Michałowska and Rapiński, 2021). With the maturity of various technologies and recognition training databases, various communities have created a batch of open source, shared, and API-callable recognition apps or platform for the public. The users only need to upload photos to get the recognized result, and the accuracy is quite good. Open source recognition tools for LiDAR results have also been developed rapidly. The accuracy of species classification methods based on structural features based on LiDAR height, intensity, and combination of height and intensity parameters can reach from 87% to 92% (You et al., 2020). Many publications have proven that the combination of LiDAR data and multispectral or hyperspectral images produces higher accuracy of species classification compared to LiDAR data alone (Michałowska and Rapiński, 2021).

Therefore, this research intends to establish a technical framework based on the LiDAR and photogrammetry carried by drones and image recognition technologies from community to identify plant species to obtain accurate BVOCs emissions. It is expect that the combination of the LiDAR accurate characterization technology of forest canopy, the ascendant accurate identification technology of tree species, and the tree-species emission factor database obtained from long-term surveys, could creates a new way to accurately quantify the biogenic emissions.

2 Methods

2.1 The Description of Workflow

The entire workflow includes the following aspects (as shown in Fig.1) : The first is the selection of drones equipped with LiDAR and high-resolution cameras; the second is the interpretation of photogrammetry results. The third part is to give the images of each tree to API-callable plant species identify platforms, and then establish a match between the interpreted tree species and the single tree species BVOCs emission factor database; the fourth step is to calculate the BVOCs emissions of the study area based on the match results and emission factors.

2.2 Study Area

The location of the provision of the work is in the coniferous and broadleaved mixed forest of the Dinghushan Forest Ecosystem Research Station of Chinese Ecosystem Research Network (CERN). Dinghu Station is located in South Subtropical Zone, belongs to Subtropical Tropical quarter wind moisturized climate, and winter and summer climate is obvious. The average annual temperature is 20.9 °C, the average annual rainfall is 1900 mm, and the annual sun radiation is about 4665 $MJ \cdot m^{-2} \cdot year^{-1}$, and the average annual sunshine time is 1433 hours, and the average annual evaporation amount is 1115 mm, and the average relative humidity in many years is 82%. The position is near the northern return line, and its elevation is 300∼350 meters while the slope is about 25°∼30°, and the slope direction is south. Its soil is Lateritic red soil, the soil layer depth is about 30 cm to 90 cm. This plot has a long-term on-site survey of tree species, which facilitates the comparison of test results. There are 260 families, 864 genus, 1740 species, and 349 species of cultivated plants in Dinghushan Forest. At the same time, Li et al. (2021) used drones equipped with online mass spectrometers at Dinghushan Station to observe the composition of VOCs. It is expect to compare their results to explore the influence of tree species on the spatial heterogeneity of VOCs.

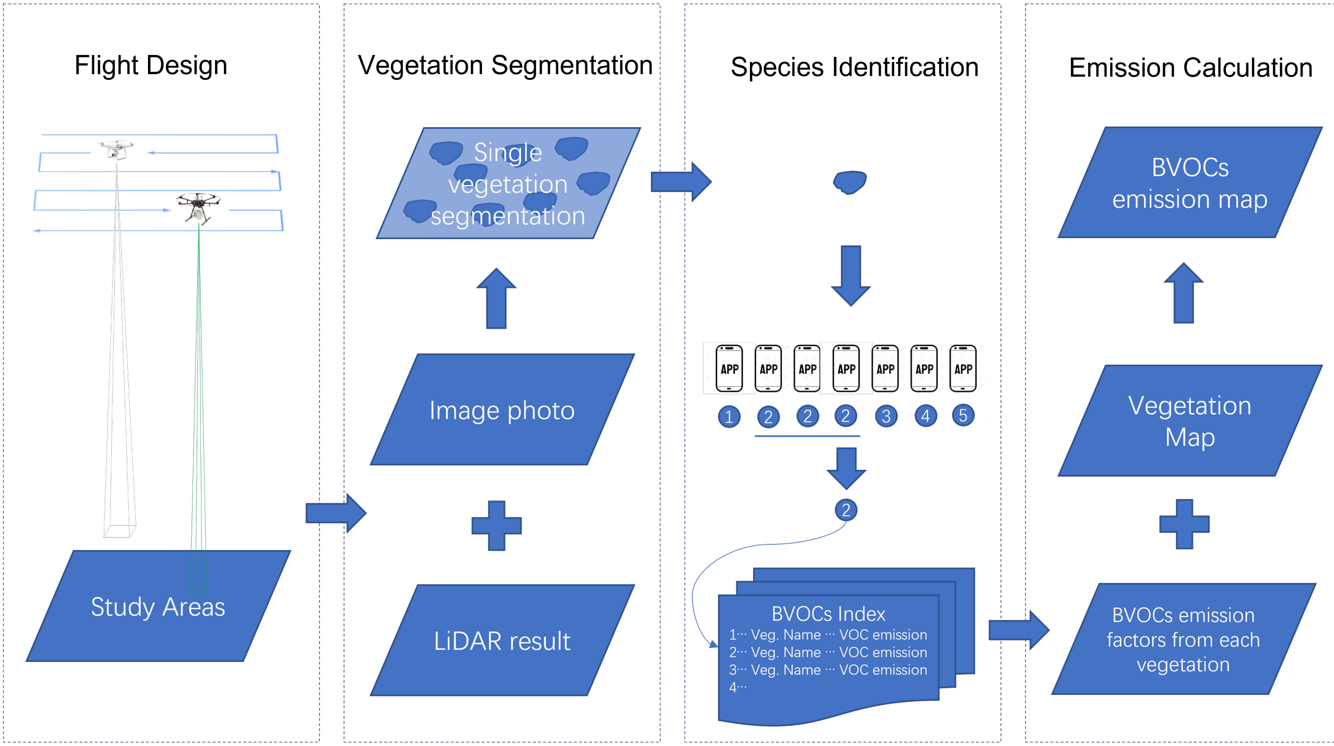

Figure 1. Schematic workflow of this study

2.3 Flight Equipment and Instruments

The main UAV platform used in this technical framework is DJI® Matrice 600 Pro, which is an universal platform that can carry various sensors. We equipped the GreenValley® LiAir V LiDAR scanning system on this platform, which includes a set of integrated navigation system composed of global navigation satellite systems(GNSS), inertial measurement unit(IMU), and attitude calculation software.

At the same time, we simultaneously used a DJI® Phantom 3 Professional UAV to get visible light images. Its camera model is FC300X_3.6_4000×3000(RGB) , and the camera image sensor (CMOS) is $1/2.3$ inch which effective pixels is 12.4 million (total pixels 12.76 million). According to the image attribute information, the camera parameters used in this work are: aperture value $f/2.8$, maximum aperture 2, exposure time $1/1250$ second, ISO speed 100, focal length 4 mm.

The DJI® pilot software are employed to design the flight route and guide the flight of the UAVs. The flight mode of the two planes is designed as a same flight route, so that they can obtain a consistent measurement area. It is worth noting that in forest areas, due to the dense layers of trees, there are significant risks during takeoff and landing, so it is usually necessary to find a suitable landing location. We usually choose the location at the "forest gap", which is usually a tomb, ridge, or other natural bare ground. At the beginning of the takeoff phase, we used manual operation to avoid trees near the forest gap to reduce the risk of a crash, while completing inertial guidance for the IMU. After the takeoff reaches the specified height, it changes to automatic flight (as shown in Fig. 2).

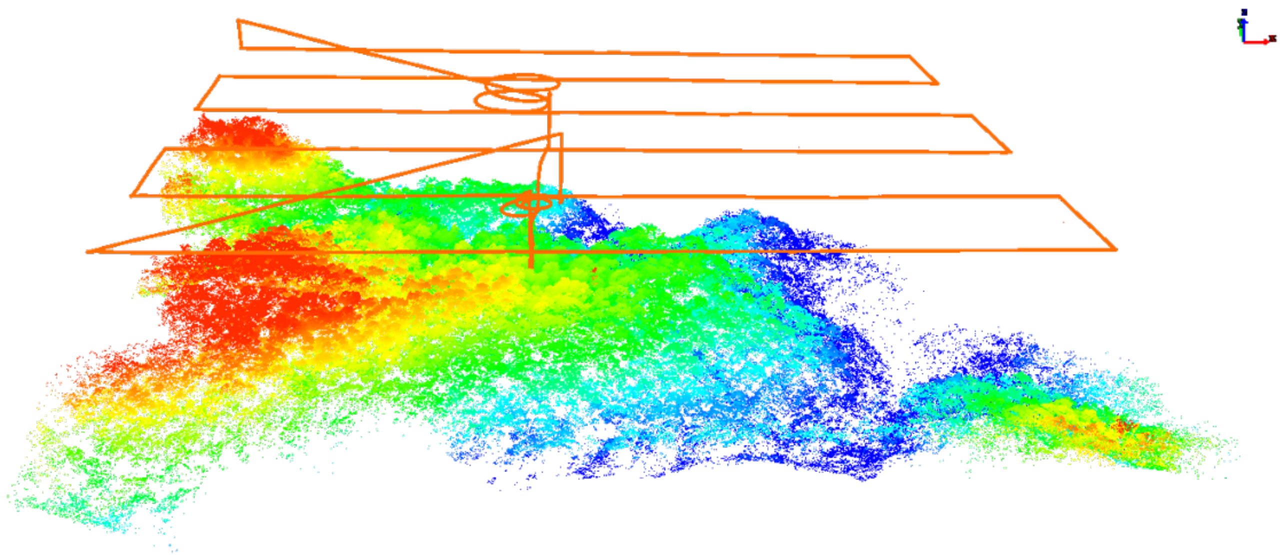

Figure 2. Flight route of this study

2.4 LiDAR-Based Tree Segmentation and Canopy Structure Calculation

The study specifically uses GreenValley® LiDAR360 and Esri® ArcGIS software to carry out this part of the work. First, the laser point cloud results are coordinated and spliced, and then the noise is removed when it overload 5 times the standard deviation, and then the improved progressive TIN densification (IPTD) algorithm is used to separate the ground points (Zhao et al., 2016). On this basis, a digital elevation model is generated based on the inverse distance weight (IDW) method (Ismail et al., 2016).

The processing of obtaining single tree features based on LiDAR is based on the layer stacking algorithm (Ayrey et al., 2017). According to the layer height of different trees, the position of the seed point in the laser point cloud is determined for segmentation, and then the boundary of each tree is obtained. The principle of this algorithm is to first obtain the seed points of each single tree and then find its watershed (Li et al., 2012). On this basis, the default calculation module of LiDAR360 is used to obtain the structural characteristic parameters of tree canopy, such as canopy height, crown radius, etc (Ma et al., 2017). At the same time, we fuse and concatenate the airborne visible light image into a complete image raster data. Based on the individual tree boundary, the results of the visible light raster data segmentation through the overlay analysis of ArcGIS are used to obtain the raster of each individual tree. The specific parameter settings for airborne image data processing are shown

Table 1. The specific parameter settings for airborne image data processing

Patameter	Value	Unit
Ground sample distance	7.2	cm
Overlap in flight direction	85%	-
Side overlap	60%	-
Aera Coverd	0.372	km^2
Mean absolute geolocation variance	0.0138-0.0361	cm
Mean point density	42.6	$point/m^2$

in the Table 1. After that, the raster of individual trees are given to different APPs to obtain the plant species identification results.

2.5 Vegetation Identification

With the continuous improvement of a new generation of plant recognition algorithms based on deep learning methods, a variety of plant recognition APPs and platforms continue to appear (Irimia et al., 2020; Otter et al., 2021). They can all import and identify plant images in the mobile phones or give a application programming interface (API) to the public researchers. There are also quite a lot of open source deep learning trained models and datasets, allowing researchers to submit visible light images and obtain recognition results (Ma et al., 2019; Zhanhui et al., 2020).

The apps and platforms shown in the Table 2 were used in this study to identify the visible light image after point cloud segmentation. They are usually trained based on a certain national or international plant classification picture database. For example, the AiPlants® is based on the database of Plant Photo Bank of China (PPBC) (Zhanhui et al., 2020). With the rise of cloud computing services, there have provided their own calling methods on various platforms, such as Aliyun® general image recognition service (GIRS), Amazon® rekognition service, Baidu® paddle-paddle platform, etc. And their identification results can be obtained using simple script submission (Jin, 2017). However, due to differences in their respective training sets, the accuracy of plant recognition varies among different apps, It is currently unclear whether the reliability, accuracy, and portability of these simple retrieval methods can support their application in investigating plant emissions. In this study, a simple recognition and judgment method was adopted to ensure our recognition accuracy. We perform a conditional judgment on all results, and if one input data obtains the same recognition result on two or more platforms, the recognition result is accepted.

2.6 BVOCs Emission Factor and Emission Calculation

In this study, we calculated based on the database of detailed BVOCs emission factors (EF) for tree species provided by MEGAN3.2 which contains a set of EF libraries with more than 40,000 tree species (Guenther et al., 2018). When the tree species determined based on section 2.5 is clear, the corresponding BVOCs EF can be obtained by looking up from the table.

Table 2. List of plant species identification apps and platforms

Name	Source	Reference
AiPlants	http://hbl.nongbangzhu.cn/	Zhanhui et al. (2020)
Aliyun GIRS	https://vision.aliyun.com/	Jin (2017)
Baidu EasyDL (PaddlePaddle)	https://cloud.baidu.com/	Ma et al. (2019)
LeafSnap	http://leafsnap.com/	Kumar et al. (2012)
$Pl@ntNet$	https://identify.plantnet.org/	Joly et al. (2016)
PlantSnap	https://www.plantsnap.com/	Otter et al. (2021)
Tree-detection-evo	https://github.com/jaeeolma/tree-detection-evo/	Mäyrä et al. (2021)

For the types of trees that are not contained in the EF library, we obtain the BVOCs emission factor of the tree species based on the literature survey method (Chen et al., 2022; Mu et al., 2022). For tree species that cannot be found even through literature research, we choose to replace them with plants from the same family. Because there are quite a few types of BVOCs obtained by observation experiments, they are generally dominated by isoprene and monoterpenes (Li et al., 2021). Therefore, our study is also characterized by the distribution of emissions using its genus-specific average emission factor.

Since the images we use to identify tree species are single temporal, we only attempt to calculate the maximum and minimum emissions of the forest in the sample plot. The calculation method is based on the emission factors corresponding to the species of each tree, multiplied by its biomass and the area occupied by its crown diameter.

3 Results

3.1 The morphological composition of the vegetation

Based on the point cloud results measured by LiDAR, more accurate arbor morphological characteristics can be obtained. Then we split the individual trees, and the point clouds of each individual tree are shown in Fig. 3. It can be seen that due to the influence of terrain, the point cloud at the edge has a much lower density than the point cloud in the center, which may cause higher uncertainty in the segmentation of the single-wood in this area.

After the statistics of single tree segmentation, there are 1291 trees in the sample plot. The overall distribution of morphological parameters and the corresponding relationship between tree height and crown diameter of each tree are shown in Fig.4. It can be seen that the tree height in the sample plot obtained by the measurement follows the GaussAmp skew distribution. Its distribution range spans from 2 m to 30 m, and its average is at 14.9 m. At the same time, its crown radius presents a lognormal distribution, and its average value is about 4 m.

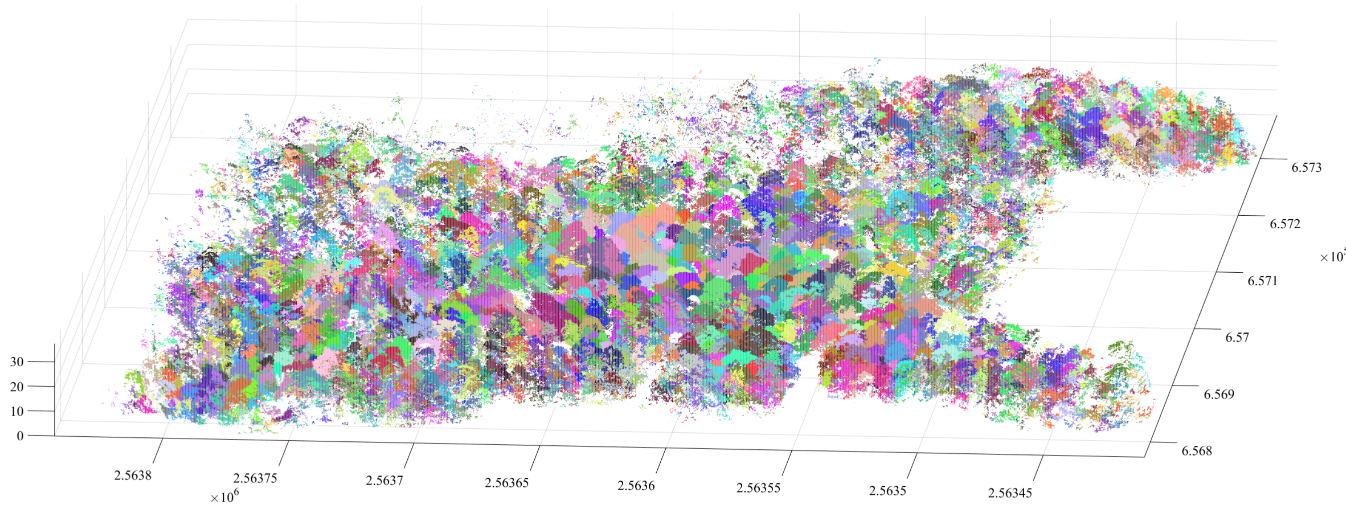

Figure 3. Point cloud of each individual tree obtained based on layer stacking algorithm excluding topographic

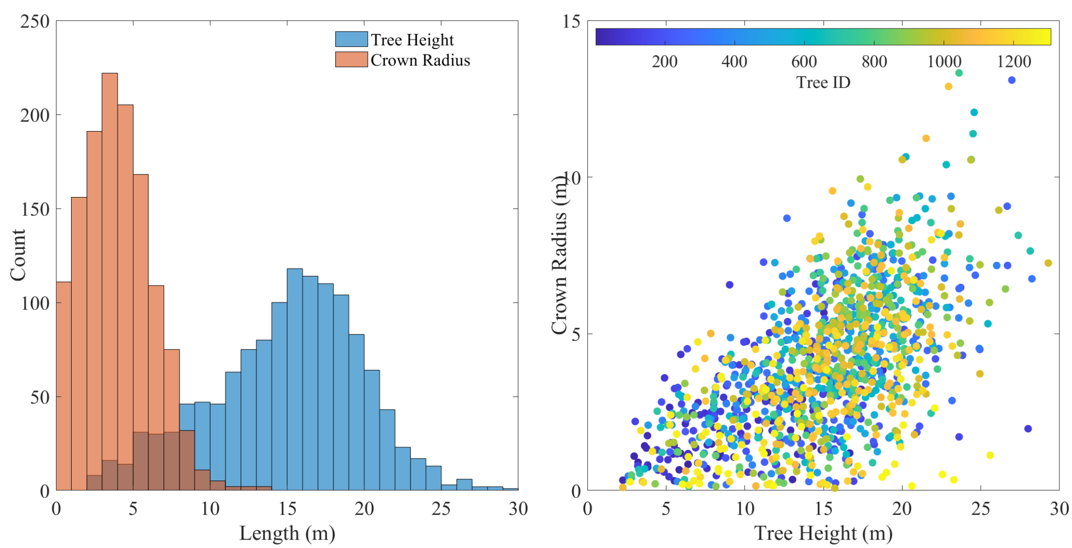

Figure 4. The distribution of tree height and crown radius (left: overall distribution; right: each tree)

3.2 The composition of vegetation species

The plant identification APPs were called to identify the tree species based on the segmentation results. The spatial distribution and frequency of tree species are shown in Fig.5 and Table 3 It can be seen from its spatial distribution that different tree species appear to be scattered and gathered. Among them, the top three frequency tree species is *Aidia canthioides (Champ. ex Benth.) Masam.*, followed by *Macaranga sampsonii Hance*, and third is *Blastus cochinchinensis Lour.* while the highest frequency family is *Euphorbiaceae*. The ratio of top three species is about 12%, 11% and 6%. Other identified tree species are also shown in Table 3. Combined with their canopy morphology distribution, it can be seen that the plot presents significant coniferous and broad-leaved mixed forest characteristics, and coniferous/broad-leaved trees occupy the position of dominant tree species. Meanwhile, it still can be see from Fig.5 that lots of trees could not recognized.

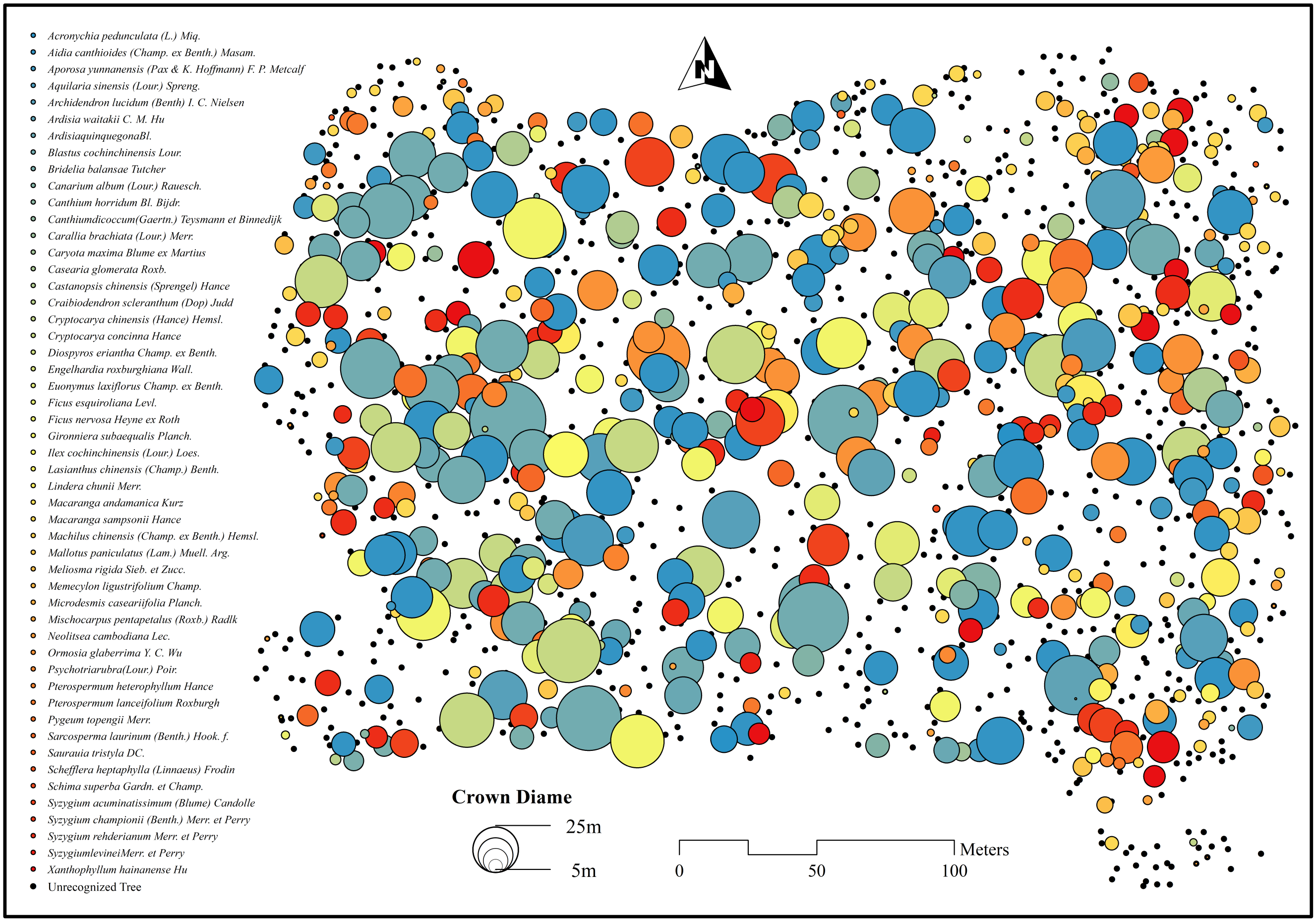

Figure 5. The spatial distribution of tree species

3.3 The BVOCs emission in family and individualized scale

The emission we obtained for isoprene and monoterpene for each family are shown in Table 4. It can be seen that in the study area of Dinghu Mountain, the largest cumulative isoprene emissions were from *Myrtaceae* family (maximum 18.7 $\mu gCm^{-2}h^{-1}$), followed by *Salicaceae* family (maximum 3.8 $\mu gCm^{-2}h^{-1}$), while for monoterpenes their cumulative emissions were largest in *Rubiaceae* family (maximum 3.9 $\mu gCm^{-2}h^{-1}$), followed by *Theaceae* family (maximum 2.8 $\mu gCm^{-2}h^{-1}$). However, it is worth noting that since we cannot confirm the leaf type, leaf age, and corresponding phenological period of each tree, we only calculated the maximum and minimum possible emissions based on their standard emission factors and biomass.

At the same time, the spatial distribution of individual plant emissions from Fig.6 shows that there are clusters of BVOCs emitting plants in the study area, which are caused by the aggregation of plants of the same family. The clusters of isoprene and terpene emitting plants are homogeneous, while there are some non-BVOCs emitting plants between the different clusters, which may be related to their ecological competition strategy (Fitzky et al., 2019). According to the forest competition theory, the emission of BVOCs is related to its competitive pressure, relative size and area overlap rate (Contreras et al., 2011). On the other hand, the strategies adopted by different species are different. The intra-specific competition and inter-specific competition play a specific role through different biopheromones which are all BVOCs (Šimpraga et al., 2019). In addition, it is noteworthy from Fig.6 that the number of plants not discriminated in the study area is quite large, implying that this is an important source of uncertainty in the estimation of BVOCs emissions in this method.

4 Discussion

4.1 The uncertainties sources of this method

4.1.1 Flight route design and aerial survey data acquisition process

During the field flight using this workflow, we found that the height of the flight and the pixel area occupied by each tree in the resulting visible light image is the decisive link that determines whether the image recognition tool can effectively identify the plant species in the image. In practice flight, we designed different flight altitude routes, namely 60 meters, 120 meters and 200 meters, in order to find a suitable flight altitude. We checked and found that for the images obtained at a flying altitude of 120 meters or more, the number of pixels per tree obtained after being cut and paired by a single tree in the LiDAR point cloud is less (about 200*300 pixels). The description of tree leaf characteristics is very unclear and presents mosaic-like characteristics, which makes it impossible to accurately identify the hidden plant species in different image recognition tools, which also makes it hard in the calculation of BVOCs emissions. Especially due to the fact that the images obtained from drone flight surveys are all orthophoto images, their expression in canopy morphology features is missing.

At the same time, the vegetation below the forest canopy also emits a considerable amount of BVOCs. Although airborne LiDAR can detect their presence through leaf gaps. visible light images cannot obtain their information due to canopy occlusion, making it an important source of underestimation of BVOCs emissions for this method. It may be possible to try using lateral aerial photography or airborne multi-band enhanced penetrating LiDAR technology to achieve detection and modeling recognition of understory plants.

4.1.2 Single tree segmentation and recognition process of images

The single tree segmentation technique used in this study is based on the layer stacking algorithm. This single tree segmentation process first obtains the seed points of each tree, and then determines the boundaries between each individual tree through its watershed (Li et al., 2012). This method may result in undetected or incorrectly detected trees, depending on the density of the laser point cloud per unit area. In this study, the density of laser point clouds was 42.6 pointm^2, which although very high, may

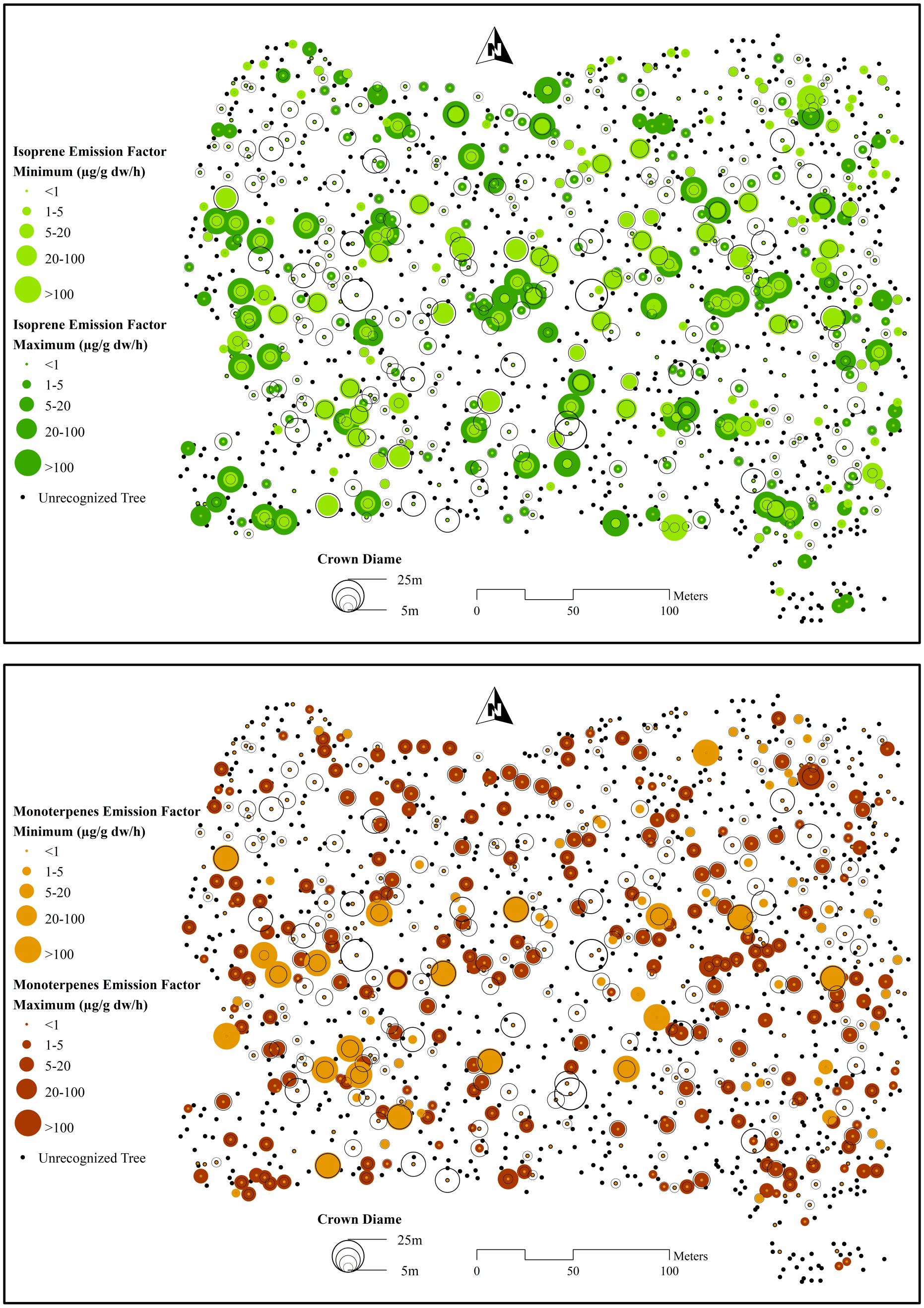

Figure 6. The individualized spatial distribution of isoprene and monoterpenes emission factor

still result in some small saplings not being correctly identified. In future research, techniques such as ground-based LiDAR segmentation and coarse-to-fine algorithms can be combined to improve its accuracy (Zhao et al., 2023).

It also can be seen that the recognition accuracy of these APPs is not as high as it claims for the visible light images obtained by drones. Among them, platforms trained by satellite images give quite accurate results of tree specie recognition. EasyDL gave back "unrecognizable" feedback for quite a lot of individual tree images while AiPlants and LeafSnap gave incorrect classification and recognition results such as succulents, garden plants, etc. This result may related to the fact that the APPs did not train image inputs with right tree species tags during the collection and training of the general image datasets.

In general, for the refined calculation of vegetation VOCs emission factors, the platform based on deep learning training from remote sensing images can provide faster and more reliable tree species identification results than traditional methods. However, these recognition platforms still require more accurate and large-scale training datasets to support their classification accuracy. Although various crowdsourcing based apps are widely used, most of the vegetation tree species information uploaded by users is concentrated in garden tree species or common tree species, more sample images are needed for rare tree species. Due to the differences of functions and selected training datasets of different platforms, it is difficult to quantify the range of uncertainty of this process. With the development of open source databases and open source training sets, further uncertainty source control of this process can be promoted.

4.1.3 The estimation process of BVOCs emissions

Although this study integrated MEGAN's emission tree species information and literature obtained information as input calculations, MEGAN mainly consists of common tree species at the global scale. Therefore, the emission factors of various tree species used in this study mainly came from Mu et al. (2022) measured results database. This literature has made it quite rare to measure over a hundred species of trees in South China, allowing for the discovery of emission factor information for most of the tree species in the sample plot of this study. But this situation indicates that there are several technical issues in selecting the BVOCs emission factor library when applying this framework. Firstly, there are still considerable cases in this study where the tree species analyzed are not within the range of the MEGAN EF database. Secondly, the emission of BVOCs from trees is subject to various photochemical and hydrothermal conditions, but currently, various databases are unable to provide detailed characterization of the impact of these environmental factors at the tree species level. Thirdly, different BVOCs emission factor databases have different emphasis on the emission parameters of BVOCs components for the same tree species. The above shortcomings limit our further application and migration of this method to other forests. However, this method can quickly obtain an independent set of upper and lower limits of BVOCs emissions for its sample plot, which is helpful for conducting model validation work based on the sample plot. It is recommended that community peers refer to our workflow and combine it with their local tree species emission factor library to further BVOCs emissions estimation.

Meanwhile, it is important for the academic community to understand that existing BVOCs computational emission models such as MEGAN have already taken into account various meteorological conditions, leaf growth, and other factors relatively completely. However, its definition of vegetation itself often depends on the definition of land use types in the coupled regional models. For example, in the commonly used WRF-Chem model, vegetation types are usually classified using the MODIS 20 or USGS 24 classification systems, which still using the combination of coniferous forests, broad-leaved forests, mixed forests, evergreen forests, and deciduous forests for forest classification. This means that there is a need for further improvement in the characterization of emissions from different tree species. Therefore, future regional estimation of BVOCs can be carried out by combining the method framework obtained in this study with the coupling of BVOCs computational emission models.

4.2 The differences of BVOCs emission from other method and its potential impact

We compared the BVOCs results obtained in this study with the emission results obtained by different methods in the Dinghu Mountain sample plot, as shown in the Table 5. It can be seen that there are many different research methods (including remote sensing inversion, model calculation, understory sampling observation, unmanned aerial vehicle mounted sensor observation, etc.), and the magnitude of the BVOC emissions from Dinghu Mountain varies greatly. The results obtained from this study indicate that a more accurate description of forest biodiversity can make the calculated results more consistent with those obtained from direct observations in the forest canopy. At the same time, it can be found that in previous model estimations based on simple PFT methods to estimate biomass, the emission of BVOCs may be underestimated to a considerable extent. This poses new requirements for the estimation and parameterization of BVOCs emissions, that is, when simulating the emission of BVOCs, the biodiversity of the forest in the region should be considered, and the consideration of vegetation factors not only comes from pure canopy physical size indicators such as LAI and crown diameter.

5 Conclusions

This research has established a workflow for identifying plant species based on LiDAR, photogrammetry and image recognition technologies carried by drones to obtain accurate BVOCs emissions. The innovation of this research is to combine the newly developed rapid survey method of plant species with the calculation of BVOCs emissions, and discussed the main uncertainty sources of the BVOCs emissions obtained in this method. The current limitation of this study is that although LiDAR can capture the multi-layer structure of tree crowns, visible light is difficult to identify other vegetation below trees, such as shrubs and herbs, which can result in a certain loss of BVOCs emissions.

The implication of this study is that, with the advancement of novel technologies in computer science, the obstacle of tree species identification, which previously impeded the estimation of BVOCs emissions, will gradually be addressed through large-scale image recognition technology. However, the open-source and standardized image recognition techniques, along with the BVOCs emission factor library for tree species, have emerged as new bottlenecks, necessitating the relevant research community to contemplate on how to share corresponding data and technologies more openly.

Author contributions. DX: Data curation, Writing – original draft preparation; MC: Supervision, Conceptualization, Methodology, Visualization, Writing – original draft preparation; GW: Data curation, Software, Validation, Visualization; SS: Formal analysis, Investigation; SZ: Resources, Drone Techniques; QZ: Data curation; YH:Writing – review & editing; WW: Writing – review & editing; WC: Writing – review & editing; BY: Writing – review & editing; XW: Project administration

Competing interests. The authors declare that they have no conflict of interest.

Acknowledgements. This work was supported by the National Key Research and Development Program of China (2023YFC3706202), the National Natural Science Foundation (42275107, 41905086, 41705123), the Science and Technology Projects in Guangzhou (2023A04J0251), the Special Fund Project for Science and Technology Innovation Strategy of Guangdong Province (Grant No.2019B121205004). The authors thank the Dinghushan Forest Ecosystem Research Station for provide sample plots.

References

Ayrey, E., Fraver, S., Kershaw Jr, J. A., Kenefic, L. S., Hayes, D., Weiskittel, A. R., and Roth, B. E.: Layer stacking: a novel algorithm for individual forest tree segmentation from LiDAR point clouds, Canadian Journal of Remote Sensing, 43, 16–27, 2017.

Baghi, R., Helmig, D., Guenther, A., Duhl, T., and Daly, R.: Contribution of flowering trees to urban atmospheric biogenic volatile organic compound emissions, Biogeosciences, 9, 3777–3785, 2012.

Batista, C. E., Ye, J., Ribeiro, I. O., Guimarães, P. C., Medeiros, A. S., Barbosa, R. G., Oliveira, R. L., Duvoisin, S., Jardine, K. J., Gu, D., et al.: Intermediate-scale horizontal isoprene concentrations in the near-canopy forest atmosphere and implications for emission heterogeneity, Proceedings of the National Academy of Sciences, 116, 19 318–19 323, 2019.

Brosy, C., Krampf, K., Zeeman, M., Wolf, B., Junkermann, W., Schäfer, K., Emeis, S., and Kunstmann, H.: Simultaneous multicopter-based air sampling and sensing of meteorological variables, Atmospheric Measurement Techniques, 10, 2773–2784, 2017.

Canaval, E., Millet, D. B., Zimmer, I., Nosenko, T., Georgii, E., Partoll, E. M., Fischer, L., Alwe, H. D., Kulmala, M., Karl, T., et al.: Rapid conversion of isoprene photooxidation products in terrestrial plants, Communications earth & environment, 1, 1–9, 2020.

Chen, W., Guenther, A. B., Wang, X., Chen, Y., Gu, D., Chang, M., Zhou, S., Wu, L., and Zhang, Y.: Regional to global biogenic isoprene emission responses to changes in vegetation from 2000 to 2015, Journal of Geophysical Research: Atmospheres, 123, 3757–3771, 2018.

Chen, W., Guenther, A. B., Jia, S., Mao, J., Yan, F., Wang, X., and Shao, M.: Synergistic effects of biogenic volatile organic compounds and soil nitric oxide emissions on summertime ozone formation in China, Science of The Total Environment, 828, 154 218, 2022.

Cheng, K., Su, Y., Guan, H., Tao, S., Ren, Y., Hu, T., Ma, K., Tang, Y., and Guo, Q.: Mapping China's planted forests using high resolution imagery and massive amounts of crowdsourced samples, ISPRS Journal of Photogrammetry and Remote Sensing, 196, 356–371, 2023.

Contreras, M. A., Affleck, D., and Chung, W.: Evaluating tree competition indices as predictors of basal area increment in western Montana forests, Forest Ecology and Management, 262, 1939–1949, 2011.

Curtis, A., Helmig, D., Baroch, C., Daly, R., and Davis, S.: Biogenic volatile organic compound emissions from nine tree species used in an urban tree-planting program, Atmospheric Environment, 95, 634–643, 2014.

Dash, J. P., Watt, M. S., Pearse, G. D., Heaphy, M., and Dungey, H. S.: Assessing very high resolution UAV imagery for monitoring forest health during a simulated disease outbreak, ISPRS Journal of Photogrammetry and Remote Sensing, 131, 1–14, 2017.

Dicke, M. and Baldwin, I. T.: The evolutionary context for herbivore-induced plant volatiles: beyond the 'cry for help', Trends in Plant Science, 15, 167–175, 2010.

Fassnacht, F. E., Latifi, H., Stereńczak, K., Modzelewska, A., Lefsky, M., Waser, L. T., Straub, C., and Ghosh, A.: Review of studies on tree species classification from remotely sensed data, Remote Sensing of Environment, 186, 64–87, 2016.

Fitzky, A. C., Sandén, H., Karl, T., Fares, S., Calfapietra, C., Grote, R., Saunier, A., and Rewald, B.: The interplay between ozone and urban vegetation—BVOC emissions, ozone deposition, and tree ecophysiology, Frontiers in Forests and Global Change, 2, 50, 2019.

Gao, X., Zhang, H., Cai, X., Song, Y., and Kang, L.: VOCs fluxes analysis based on micrometeorological methods over litchi plantation in the Pearl River Delta, China, Acta Scientiarum Naturalium Universitatis Pekinensis, 47, 916–922, 2011.

Ghirardo, A., Xie, J., Zheng, X., Wang, Y., Grote, R., Block, K., Wildt, J., Mentel, T., Kiendler-Scharr, A., Hallquist, M., et al.: Urban stress-induced biogenic VOC emissions and SOA-forming potentials in Beijing, Atmospheric Chemistry and Physics, 16, 2901–2920, 2016.

Guenther, A., Jiang, X., Heald, C. L., Sakulyanontvittaya, T., Duhl, T., Emmons, L., and Wang, X.: The Model of Emissions of Gases and Aerosols from Nature version 2.1 (MEGAN2. 1): an extended and updated framework for modeling biogenic emissions, Geoscientific Model Development, 5, 1471–1492, 2012.

Guenther, A., Jiang, X., Shah, T., Huang, L., Kemball-Cook, S., and Yarwood, G.: Model of Emissions of Gases and Aerosol from Nature Version 3 (MEGAN3) for Estimating Biogenic Emissions, International Technical Meeting on Air Pollution Modelling and its Application, pp. 187–192, 2018.

Hartley, A., MacBean, N., Georgievski, G., and Bontemps, S.: Uncertainty in plant functional type distributions and its impact on land surface models, Remote Sensing of Environment, 203, 71–89, 2017.

Heald, C. L. and Kroll, J.: The fuel of atmospheric chemistry: Toward a complete description of reactive organic carbon, Science Advances, 6, eaay8967, 2020.

Henze, D., Seinfeld, J., Ng, N., Kroll, J., Fu, T.-M., Jacob, D. J., and Heald, C.: Global modeling of secondary organic aerosol formation from aromatic hydrocarbons: high-vs. low-yield pathways, Atmospheric Chemistry and Physics, 8, 2405–2420, 2008.

Irimia, C., Costandache, M., Matei, M., and Lipan, M.: Discover the Wonderful World of Plants with the Help of Smart Devices, in: RoCHI-INTERNATIONAL CONFERENCE ON HUMAN-COMPUTER INTERACTION, p. 73, 2020.

Isidorov, V., Zenkevich, I., and Ioffe, B.: Volatile organic compounds in solfataric gases, Journal of Atmospheric Chemistry, 10, 329–340, 1990.

Ismail, Z., Abdul Khanan, M., Omar, F., Abdul Rahman, M., and Mohd Salleh, M.: Evaluating error of lidar derived dem interpolation for vegetation area, International Archives of the Photogrammetry, Remote Sensing & Spatial Information Sciences, 42, 2016.

Jin, R.: Deep Learning at Alibaba., in: Twenty-Sixth International Joint Conference on Artificial Intelligence, pp. 11–16, 2017.

Jin, S., Sun, X., Wu, F., Su, Y., Li, Y., Song, S., Xu, K., Ma, Q., Baret, F., Jiang, D., et al.: Lidar sheds new light on plant phenomics for plant breeding and management: Recent advances and future prospects, ISPRS Journal of Photogrammetry and Remote Sensing, 171, 202–223, 2021.

Joly, A., Bonnet, P., Goëau, H., Barbe, J., Selmi, S., Champ, J., Dufour-Kowalski, S., Affouard, A., Carré, J., Molino, J.-F., Boujemaa, N., and Barthélémy, D.: A look inside the Pl@ntNet experience, Multimedia Systems, 22, 751–766, 2016.

Kegge, W. and Pierik, R.: Biogenic volatile organic compounds and plant competition, Trends in Plant Science, 15, 126–132, 2010.

Komenda, M. and Koppmann, R.: Monoterpene emissions from Scots pine (Pinus sylvestris): field studies of emission rate variabilities, Journal of Geophysical Research: Atmospheres, 107, ACH–1, 2002.

Kumar, N., Belhumeur, P. N., Biswas, A., Jacobs, D. W., Kress, W. J., Lopez, I., and Soares, J. V. B.: Leafsnap: A Computer Vision System for Automatic Plant Species Identification, in: The 12th European Conference on Computer Vision (ECCV), 2012.

Laothawornkitkul, J., Taylor, J. E., Paul, N. D., and Hewitt, C. N.: Biogenic volatile organic compounds in the Earth system, New Phytologist, 183, 27–51, 2009.

Li, W., Guo, Q., Jakubowski, M. K., and Kelly, M.: A new method for segmenting individual trees from the lidar point cloud, Photogrammetric Engineering & Remote Sensing, 78, 75–84, 2012.

Li, Y., Liu, B., Ye, J., Jia, T., Khuzestani, R. B., Sun, J. Y., Cheng, X., Zheng, Y., Li, X., Wu, C., et al.: Unmanned Aerial Vehicle Measurements of Volatile Organic Compounds over a Subtropical Forest in China and Implications for Emission Heterogeneity, ACS Earth and Space Chemistry, 5, 247–256, 2021.

Loreto, F., Dicke, M., SCHNITZLER, J.-P., and Turlings, T. C.: Plant volatiles and the environment, Plant, Cell & Environment, 37, 1905–1908, 2014.

Ma, Q., Su, Y., and Guo, Q.: Comparison of canopy cover estimations from airborne LiDAR, aerial imagery, and satellite imagery, IEEE Journal of Selected Topics in Applied Earth Observations and Remote Sensing, 10, 4225–4236, 2017.

Ma, Y., Yu, D., Wu, T., and Wang, H.: PaddlePaddle: An open-source deep learning platform from industrial practice, Frontiers of Data and Domputing, 1, 105–115, 2019.

Mäyrä, J., Keski-Saari, S., Kivinen, S., Tanhuanpää, T., Hurskainen, P., Kullberg, P., Poikolainen, L., Viinikka, A., Tuominen, S., Kumpula, T., et al.: Tree species classification from airborne hyperspectral and LiDAR data using 3D convolutional neural networks, Remote Sensing of Environment, 256, 112 322, 2021.

Mellouki, A., Wallington, T., and Chen, J.: Atmospheric chemistry of oxygenated volatile organic compounds: impacts on air quality and climate, Chemical reviews, 115, 3984–4014, 2015.

Michałowska, M. and Rapiński, J.: A Review of Tree Species Classification Based on Airborne LiDAR Data and Applied Classifiers, Remote Sensing, 13, 353, 2021.

Mu, Z., Llusià, J., Zeng, J., Zhang, Y., Asensio, D., Yang, K., Yi, Z., Wang, X., and Peñuelas, J.: An Overview of the Isoprenoid Emissions From Tropical Plant Species, Frontiers in plant science, 13, 1–14, 2022.

Nebiker, S., Annen, A., Scherrer, M., and Oesch, D.: A light-weight multispectral sensor for micro UAV—Opportunities for very high resolution airborne remote sensing, Int. Arch. Photogramm. Remote Sens. Spat. Inf. Sci, 37, 1193–1200, 2008.

Otter, J., Mayer, S., and Tomaszewski, C. A.: Swipe Right: a Comparison of Accuracy of Plant Identification Apps for Toxic Plants., Journal of Medical Toxicology, 17, 42–47, 2021.

Peñuelas, J. and Staudt, M.: BVOCs and global change, Trends in Plant Science, 15, 133–144, 2010.

Ran, L., Zhao, C., Xu, W., Lu, X., Han, M., Lin, W., Yan, P., Xu, X., Deng, Z., Ma, N., et al.: VOC reactivity and its effect on ozone production during the HaChi summer campaign, Atmospheric Chemistry and Physics, 11, 4657–4667, 2011.

Rüdiger, J., Tirpitz, J.-L., Moor, J., Bobrowski, N., Gutmann, A., Liuzzo, M., Ibarra, M., and Hoffmann, T.: Implementation of electrochemical, optical and denuder-based sensors and sampling techniques on UAV for volcanic gas measurements: Examples from Masaya, Turrialba and Stromboli volcanoes, Atmospheric Measurement Techniques, 11, 2441–2457, 2018.

Sarkar, C., Guenther, A. B., Park, J.-H., Seco, R., Alves, E., Batalha, S., Santana, R., Kim, S., Smith, J., Tóta, J., et al.: PTR-TOF-MS eddy covariance measurements of isoprene and monoterpene fluxes from an eastern Amazonian rainforest, Atmospheric Chemistry and Physics, 20, 7179–7191, 2020.

Schneider, F. D., Morsdorf, F., Schmid, B., Petchey, O. L., Hueni, A., Schimel, D. S., and Schaepman, M. E.: Mapping functional diversity from remotely sensed morphological and physiological forest traits, Nature communications, 8, 1–12, 2017.

Shakhatreh, H., Sawalmeh, A. H., Al-Fuqaha, A., Dou, Z., Almaita, E., Khalil, I., Othman, N. S., Khreishah, A., and Guizani, M.: Unmanned aerial vehicles (UAVs): A survey on civil applications and key research challenges, Ieee Access, 7, 48 572–48 634, 2019.

Šimpraga, M., Takabayashi, J., and Holopainen, J. K.: Language of plants: where is the word?, Journal of Integrative Plant Biology, 58, 343–349, 2016.

Šimpraga, M., Ghimire, R. P., Van Der Straeten, D., Blande, J. D., Kasurinen, A., Sorvari, J., Holopainen, T., Adriaenssens, S., Holopainen, J. K., and Kivimäenpää, M.: Unravelling the functions of biogenic volatiles in boreal and temperate forest ecosystems, European Journal of Forest Research, 138, 763–787, 2019.

Simpson, J. and McPherson, E.: The tree BVOC index, Environmental Pollution, 159, 2088–2093, 2011.

Situ, S., Guenther, A., Wang, X., Jiang, X., Turnipseed, A., Wu, Z., and Bai, J.: Impacts of seasonal and regional variability in biogenic VOC emissions on surface ozone in the Pearl River delta region, China, Atmospheric Chemistry and Physics, 13, 11 803–11 817, 2013.

Situ, S., Wang, X., Guenther, A., Zhang, Y., Wang, X., Huang, M., Fan, Q., and Xiong, Z.: Uncertainties of isoprene emissions in the MEGAN model estimated for a coniferous and broad-leaved mixed forest in Southern China, Atmospheric Environment, 98, 105–110, 2014.

Steinbrecher, R., Smiatek, G., Köble, R., Seufert, G., Theloke, J., Hauff, K., Ciccioli, P., Vautard, R., and Curci, G.: Intra-and inter-annual variability of VOC emissions from natural and semi-natural vegetation in Europe and neighbouring countries, Atmospheric Environment, 43, 1380–1391, 2009.

Sylvain, J.-D., Drolet, G., and Brown, N.: Mapping dead forest cover using a deep convolutional neural network and digital aerial photography, ISPRS Journal of Photogrammetry and Remote Sensing, 156, 14–26, 2019.

Tang, J., Chan, L., Chan, C., Li, Y., Chang, C., Liu, S., Wu, D., and Li, Y.: Characteristics and diurnal variations of NMHCs at urban, suburban, and rural sites in the Pearl River Delta and a remote site in South China, Atmospheric Environment, 41, 8620–8632, https://doi.org/https://doi.org/10.1016/j.atmosenv.2007.07.029, 2007.

Tsimpidi, A. P., Trail, M., Hu, Y., Nenes, A., and Russell, A. G.: Modeling an air pollution episode in northwestern United States: Identifying the effect of nitrogen oxide and volatile organic compound emission changes on air pollutants formation using direct sensitivity analysis, Journal of the Air & Waste Management Association, 62, 1150–1165, 2012.

Villa, T. F., Gonzalez, F., Miljievic, B., Ristovski, Z. D., and Morawska, L.: An overview of small unmanned aerial vehicles for air quality measurements: Present applications and future prospectives, Sensors, 16, 1072, 2016.

Wang, H., Wu, Q., Guenther, A. B., Yang, X., Wang, L., Xiao, T., Li, J., Feng, J., Xu, Q., and Cheng, H.: A long-term estimation of biogenic volatile organic compound (BVOC) emission in China from 2001–2016: the roles of land cover change and climate variability, Atmospheric Chemistry and Physics, 21, 4825–4848, 2021.

Wang, X., Situ, S., Chen, W., Zheng, J., Guenther, A., Fan, Q., and Chang, M.: Numerical model to quantify biogenic volatile organic compound emissions: The Pearl River Delta region as a case study, Journal of Environmental Sciences, 46, 72–82, 2016.

Wu, C., Liu, B., Wu, D., Yang, H., Mao, X., Tan, J., Liang, Y., Sun, J. Y., Xia, R., Sun, J., et al.: Vertical profiling of black carbon and ozone using a multicopter unmanned aerial vehicle (UAV) in urban Shenzhen of South China, Science of The Total Environment, 801, 149 689, 2021.

Wu, F., Yu, Y., Sun, J., Zhang, J., Wang, J., Tang, G., and Wang, Y.: Characteristics, source apportionment and reactivity of ambient volatile organic compounds at Dinghu Mountain in Guangdong Province, China, Science of The Total Environment, 548-549, 347–359, https://doi.org/https://doi.org/10.1016/j.scitotenv.2015.11.069, 2016.

Wu, K., Yang, X., Chen, D., Gu, S., Lu, Y., Jiang, Q., Wang, K., Ou, Y., Qian, Y., Shao, P., et al.: Estimation of biogenic VOC emissions and their corresponding impact on ozone and secondary organic aerosol formation in China, Atmospheric Research, 231, 104 656, 2020.

You, H., Lei, P., Li, M., and Ruan, F.: Forest Species Classification Based on Three-dimensional Coordinate and Intensity Information of Airborne LiDAR Data with Random Forest Method, The International Archives of Photogrammetry, Remote Sensing and Spatial Information Sciences, 42, 117–123, 2020.

Zhanhui, X., Shiyao, L., Ying, Z., Wenqin, T., Zhaofeng, C., Entao, Z., Jing, G., Di, Z., Jun, G., Gaoying, G., Chunpeng, G., Lulu, G., Jing, W., Chunyang, X., Chuan, P., Teng, Y., Mengqi, C., Weicheng, S., Jiantan, Z., Haotian, L., Chaoqun, B., Heqi, W., Jingchao, J., Jinzhou, W., Cui, X., and Keping, M.: Evaluation of the identification ability of eight commonly used plant identification application softwares in China, Biodiversity Science, 28, 524, 2020.

Zhao, X., Guo, Q., Su, Y., and Xue, B.: Improved progressive TIN densification filtering algorithm for airborne LiDAR data in forested areas, ISPRS Journal of Photogrammetry and Remote Sensing, 117, 79–91, 2016.

Zhao, Y., Im, J., Zhen, Z., and Zhao, Y.: Towards accurate individual tree parameters estimation in dense forest: optimized coarse-to-fine algorithms for registering UAV and terrestrial LiDAR data, Giscience & remote sensing, 60, 2197 281, 2023.

Table 3. Specific species composition information of vegetation identification result

Families	Gemera	Species	Count	Mean Height (m)	Mean Crown Radius (m)
Actinidiaceae	Saurauia	Saurauia tristyla DC.	3	7.4	0.9
Aquifoliaceae	Ilex	Ilex cochinchinensis (Lour.) Loes.	1	17.2	6.7
Araliaceae	Schefflera	Schefflera heptaphylla (Linnaeus) Frodin	5	10.1	2.9
Arecaceae	Caryota	Caryota maxima Blume ex Martius	2	13.7	2.7
Burseraceae	Canarium	Canarium album (Lour.) Rauesch.	6	19.8	4.5
Cannabaceae	Gironniera	Gironniera subaequalis Planch.	19	18.0	5.6
Celastraceae	Euonymus	Euonymus laxiflorus Champ. ex Benth.	2	15.1	3.7
Ebenaceae	Diospyros	Diospyros eriantha Champ. ex Benth.	3	10.9	2.1
Ericaceae	Craibiodendron	Craibiodendron scleranthum (Dop) Judd.	2	10.6	1.6
Euphorbiaceae	Macaranga	Macaranga sampsonii Hance	67	12.5	1.9
		Macaranga andamanica Kurz	4	9.4	0.3
	Mallotus	Mallotus paniculatus (Lam.) Muell. Arg.	22	12.3	2.7
Fabaceae	Ormosia	Ormosia glaberrima Y. C. Wu	20	17.8	5.4
	Archidendron	Archidendron lucidum (Benth) I. C. Nielsen	6	18.2	7.6
Fagaceae	Castanopsis	Castanopsis chinensis (Sprengel) Hance	6	15.9	5.0
Juglandaceae	Engelhardtia	Engelhardia roxburghiana Wall.	3	11.1	2.8
Lauraceae	Cryptocarya	Cryptocarya concinna Hance	17	18.2	7.2
		Cryptocarya chinensis (Hance) Hemsl.	9	11.2	0.8
	Lindera	Lindera chunii Merr.	5	17.7	5.8
	Machilus	Machilus chinensis (Champ. ex Benth.) Hemsl.	3	12.6	3.6
	Neolitsea	Neolitsea cambodiana Lec.	1	15.1	5.5
Malvaceae	Pterospermum	Pterospermum lanceifolium Roxburgh	19	12.0	2.4
		Pterospermum heterophyllum Hance	4	15.2	3.6
Melastomataceae	Blastus	Blastus cochinchinensis Lour.	35	18.9	6.8
	Memecylon	Memecylon ligustrifolium Champ.	2	6.2	1.9
Moraceae	Ficus	Ficus esquiroliana Levl.	9	18.1	5.7
		Ficus nervosa Heyne ex Roth	2	5.6	1.8
Myrtaceae	Syzygium	Syzygium rehderianum Merr. et Perry	29	15.6	3.7
		Syzygium acuminatissimum (Blume) Candolle	10	15.3	5.5
		SyzygiumlevineiMerr. et Perry	2	9.3	2.8
		Syzygium championii (Benth.) Merr. et Perry	1	18.1	4.8
Pandaceae	Microdesmis	Microdesmis caseariifolia Planch.	6	14.0	3.2
Phyllanthaceae	Aporosa	Aporosa yunnanensis (Pax & K. Hoffmann) F. P. Metcalf	34	13.2	2.8
	Bridelia	Bridelia balansae Tutcher	4	13.2	3.8
Polygalaceae	Xanthophyllum	Xanthophyllum hainanense Hu	15	16.9	3.8
Primulaceae	Ardisia	Ardisia quinquegona Bl.	13	16.2	4.1
		Ardisia waitakii C. M. Hu	3	15.2	6.3
Rhizophoraceae	Carallia	Carallia brachiata (Lour.) Merr.	2	15.4	3.1
Rosaceae	Pygeum	Pygeum topengii Merr.	7	13.2	4.9
Rubiaceae	Aidia	Aidia canthioides (Champ. ex Benth.) Masam.	68	17.1	5.6
	Lasianthus	Lasianthus chinensis (Champ.) Benth.	6	13.0	2.8
	Peponidium	Canthium horridum Bl. Bijdr.	5	11.7	1.0
	Psychotria	Psychotria rubra (Lour.) Poir.	5	14.1	2.1
	Canthium	Canthium dicoccum(Gaertn.) Teysmann et Binnedijk	3	12.6	2.7
Rutaceae	Acronychia	Acronychia pedunculata (L.) Miq.	2	17.2	4.0
Sabiaceae	Meliosma	Meliosma rigida Sieb. et Zucc.	3	9.2	2.8
Salicaceae	Casearia	Casearia glomerata Roxb.	2	13.9	0.8
Sapindaceae	Mischocarpus	Mischocarpus pentapetalus (Roxb.) Radlk	24	11.8	1.2
Sapotaceae	Sarcosperma	Sarcosperma laurinum (Benth.) Hook. f.	8	16.9	3.7
Theaceae	Schima	Schima superba Gardn. et Champ.	3	7.8	0.7
Thymelaeaceae	Aquilaria	Aquilaria sinensis (Lour.) Spreng.	2	17.2	7.8

Table 4. The maximum and minimum emissions from different families in study area (Unit: $\mu g C m^{-2} h^{-1}$))

Families	Isoprene		Monoterpenes		Count of trees
	Minimum	Maximum	Minimum	Maximum	
Actinidiaceae	0.0	0.0	0.0	0.0	3
Aquifoliaceae	0.0	0.0	0.0	0.0	1
Araliaceae	0.0	0.0	0.0	0.0	5
Arecaceae	1.6	1.6	0.0	0.0	2
Burseraceae	0.1	2.9	0.0	0.0	6
Cannabaceae	0.0	0.0	0.0	0.0	19
Celastraceae	0.0	0.0	0.0	0.0	2
Ebenaceae	0.0	0.0	0.0	0.1	3
Ericaceae	0.0	0.0	0.0	0.0	2
Euphorbiaceae	0.6	0.9	0.1	0.1	93
Fabaceae	0.8	0.8	0.2	0.2	26
Fagaceae	0.0	0.0	0.0	0.0	6
Juglandaceae	0.0	0.0	0.0	0.0	3
Lauraceae	2.2	2.8	2.4	2.6	35
Malvaceae	0.0	0.0	0.0	0.0	23
Melastomataceae	0.0	0.0	0.0	0.0	37
Moraceae	0.1	0.4	0.0	0.0	11
Myrtaceae	0.7	18.7	0.0	0.8	42
Pandaceae	0.0	0.0	0.0	0.0	6
Phyllanthaceae	0.0	0.0	0.0	0.5	38
Polygalaceae	0.0	0.0	0.0	0.0	15
Primulaceae	0.0	0.0	0.0	0.1	16
Rhizophoraceae	0.0	0.0	0.0	0.0	2
Rosaceae	0.0	0.0	0.0	0.0	7
Rubiaceae	0.0	0.3	0.0	3.9	87
Rutaceae	0.0	0.0	0.0	0.1	2
Sabiaceae	0.0	0.0	0.0	0.0	3
Salicaceae	0.7	3.8	0.0	0.0	2
Sapindaceae	0.0	2.9	0.0	0.7	24
Sapotaceae	0.0	1.8	0.0	0.0	8
Theaceae	0.0	0.0	2.8	2.8	3
Thymelaeaceae	0.0	0.0	0.0	0.0	2
Total	**7.0**	**37.1**	**5.8**	**12.1**	**534**

Table 5. Measurements and simulations of isoprene and monoterpenes emissions/concentrations using different methods at the same site

Methods	Isoprene	Monoterpene	Reference
This study	7.0∼37.1 $\mu gCm^{-2}h^{-1}$	5.8∼12.1 $\mu gCm^{-2}h^{-1}$	-
MEGAN	0.1∼10 $\mu gCm^{-2}h^{-1}$	0.1∼10 $\mu gCm^{-2}h^{-1}$	(Guenther et al., 2012)
REA techniques	0.11 $mgCm^{-2}h^{-1}$	0.24 $mgCm^{-2}h^{-1}$	(Gao et al., 2011)
REA techniques	0.215 $mgCm^{-2}h^{-1}$	0.313 $mgCm^{-2}h^{-1}$	(Situ et al., 2013)
GC-MS	0.12 ± 0.80 ppbv	0.32 ± 0.16 ppbv (α-pinene)	(Tang et al., 2007)
GC-MS	0.76 ± 0.50 ppbv	0.33 ± 0.18 ppbv (α-pinene)	(Wu et al., 2016)
UAV-based VOC sampler	0.047 ± 0.040 ppbv	0.084 ± 0.104 ppbv (α-pinene)	(Li et al., 2021)